Bloch dynamics in lattices with long-range hopping

J. Stockhofe[1,*] and P. Schmelcher[1,2]

[1]*Zentrum für Optische Quantentechnologien, Universität Hamburg, Luruper Chaussee 149, 22761 Hamburg, Germany*

[2]*The Hamburg Centre for Ultrafast Imaging, Universität Hamburg, Luruper Chaussee 149, 22761 Hamburg, Germany*

(Received 11 November 2014; published 9 February 2015)

We study a discrete Schrödinger equation with arbitrary long-range hopping terms under the influence of an external force. The impact of long-range hoppings on the single-particle Bloch dynamics in the lattice is investigated. A closed expression for the propagator is given, based on which we analyze the dynamics of initially Gaussian wave packets. Our findings capture the anharmonic oscillations recently observed in zigzag lattices and furthermore provide a detailed quantitative description of the crossover between center-of-mass Bloch oscillations for wide wave packets and left-right symmetric width oscillations for narrow single-site excitations. The analytical results are shown to be in agreement with numerical simulations. A helix lattice setup for ultracold atoms is proposed where such hopping terms to far neighbors can be experimentally tuned to sizable values.

DOI: 10.1103/PhysRevA.91.023606 PACS number(s): 03.75.Lm, 67.85.Hj, 42.79.Gn

I. INTRODUCTION

One of the intriguing features of quantum mechanics in lattice systems is the Bloch oscillation of a particle subjected to a constant external force [1,2]. The technical advance of recent years has made it possible to prepare quantum systems clean enough to directly observe this phenomenon, and Bloch oscillation dynamics has been verified in semiconductor superlattices [3] (see [4] for a review), for ultracold atoms subject to optical lattices [5,6], and in photonic waveguide systems [7–9], among others. Nowadays, Bloch oscillation based methods are routinely used in cold-atom applications, e.g., for precision measurements of the fine-structure constant [10] or gravitational forces [11,12], even on very small length scales [13].

The discrete Schrödinger lattice model which exhibits Bloch oscillation dynamics under a constant force arises in many different areas of research, both in physics and beyond [14]. Traditionally, this dynamical model has been studied mostly within the nearest-neighbor approximation, which is sufficiently accurate in many cases. Recent years have seen an increased interest in extensions of the model where this approximation is relaxed and long-range hoppings (sometimes also termed "couplings," depending on the context) are taken into account. For instance, long-range hopping terms have been suggested to be relevant for the dynamics of the DNA molecule [15,16] (recently reviewed in [17]) or for excitation transfer in large molecules [18], superlattice structures with sizable second-neighbor hoppings have been proposed [19], and zigzag arrangements of photonic waveguides have been demonstrated as an efficient way to artificially enhance the second-neighbor hopping term in a controlled way [20]. Nonlinear features of this zigzag model have been studied theoretically [21–23] and experimentally [24]. In [25] it was proposed that the second-neighbor hopping crucially alters the Bloch oscillation dynamics, and this was confirmed in the experiment [26]. A general theoretical framework that captures all these phenomena has not been given, although crucial building blocks are known. In [27], the propagator for a force-free lattice with arbitrary long-range hoppings is derived, and in [28] general results for its diffusive dynamics are provided. Complementing this, the propagator in the presence of a constant force has been derived in [29], but restricting to short-range hoppings. There has also been a lot of interest in driven lattice systems (where the force is time dependent), and also in this context some findings beyond the nearest-neighbor approximation are available, e.g.. [30–32].

In this work, we extend these results in two ways. First, we derive the propagator for a homogeneous one-dimensional discrete Schrödinger lattice with arbitrary long-range hoppings under the influence of a constant external force. Second, we employ this propagator to systematically study the dynamics of a wave packet depending on its initial width. Restricting to a nearest-neighbor model, a first step in this direction has been done recently in [33]. It is well known (and has been observed in experiments) that for sufficiently wide wave packets the semiclassical picture of Bloch oscillations of the center-of-mass coordinate applies. In the other extreme limit, where the wave packet is so narrow that it effectively only excites a single site initially, the dynamics is completely different: Under the influence of the force, the width of the wave packet oscillates at the Bloch period while its center of mass remains at rest (see, e.g., [34]). This periodic wave-packet reconstruction goes under different names in the literature, and we will refer to it as *Bloch breathing* in the following. Following, we will give a detailed analysis of the crossover between Bloch breathing dynamics of initially narrow wave packets and Bloch oscillation dynamics of initially wide ones, taking into account the full set of long-range hopping terms.

Our study of long-range hopping models is motivated by a generalization of the zigzag lattice geometry possible in the framework of cold atoms. In the photonic waveguide systems, one of the three spatial coordinates enters the equation of motion as a time variable [35]. Thus, there are effectively only two spatial degrees of freedom for the lattice layout. In contrast, trapping potentials for cold atoms can be designed in all three spatial dimensions. We suggest a helical arrangement of lattice sites which makes it possible to enhance arbitrary long-range hopping terms (even beyond the second-nearest neighbor). A similar helix model has been briefly considered for fermions in [36,37].

*jstockho@physnet.uni-hamburg.de

The paper is structured as follows: In Sec. II, we describe the helix lattice setup that motivates our study of long-range hopping models. Section III introduces the discrete Schrödinger model we consider and lists a number of results for the force-free case. Taking into account the external force, we construct the Wannier-Stark basis and the direct space representation of the propagator in Sec. IV. Based on this propagator, we study the crossover between Bloch breathing and Bloch oscillations in Sec. V. Section VI contains a brief summary and an outlook.

II. HELIX LATTICE MODEL

Zigzag lattice geometries have been successfully used to artificially enhance the second-neighbor hopping in planar lattices. In the following, we describe a generalization of this idea that makes it possible to enhance also higher-order hoppings, at the price of not restricting to planar setups. The scheme we describe relies on the possibility of trapping ultracold atoms on helical space curves, as has been proposed recently [38,39]. A single strand helix curve is parametrized by $\vec{r}(\varphi) = (R\cos\varphi, R\sin\varphi, b\varphi)$ with R the helix radius and $2\pi b$ the helix pitch. Now let us consider potential wells located along the helix equidistantly in arc length (or, equivalently, in the angle parameter φ), i.e., the lth potential well is centered at

$$\vec{r}_l = (R\cos(l\varphi_0), R\sin(l\varphi_0), b\varphi_0 l) \tag{1}$$

for some fixed φ_0. Then, due to the special features of the helix geometry [40,41], the three-dimensional Euclidean distance between sites j and l only depends on the index difference $|j-l|$. Measured in units of the radius R, it is given by

$$\begin{aligned} d^2_{|j-l|} &= \frac{|\vec{r}_j - \vec{r}_l|^2}{R^2} \\ &= 2\{1-\cos[\varphi_0(j-l)]\} + \frac{b^2}{R^2}\varphi_0^2(j-l)^2. \end{aligned} \tag{2}$$

Interestingly, depending on the helix parameters, d_n can be a nonmonotonous function of n. This is illustrated in Fig. 1(a) which shows d_n for a helix lattice with parameters $b/R = 0.22$ and $\varphi_0 = \pi/2$. A helix of this geometry is shown in Fig. 1(c), with circular black markers indicating the lattice sites. For this particular geometry, it can be seen that the fourth neighbor (when counted along the helix) of each site is again particularly close to that site in three-dimensional space, although it is far away in index (or in arc length).

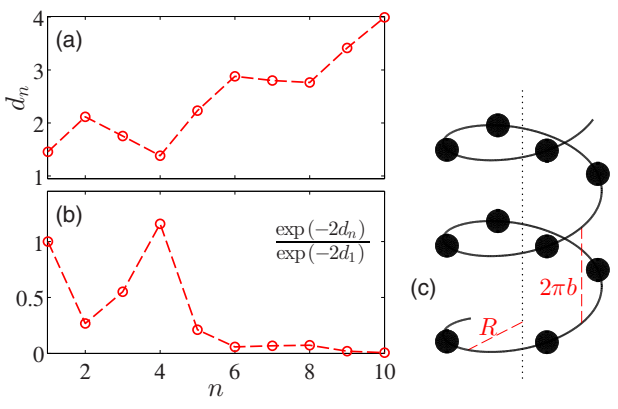

FIG. 1. (Color online) (a) Euclidean distances (in units of R) to the nth neighbor site and (b) simple exponential estimate of the scaling of the hopping amplitudes for the helix lattice model schematically shown in (c).

Let us assume now that the dynamics of quantum particles on such an infinitely extended helix lattice can be described by a noninteracting single-band Hubbard model of the form [42,43]

$$\hat{H} = \sum_{l=-\infty}^{\infty}\left[-\sum_{\alpha=1}^{\infty} t_\alpha(\hat{a}_l^\dagger \hat{a}_{l+\alpha} + \hat{a}_{l+\alpha}^\dagger \hat{a}_l) + V_l \hat{a}_l^\dagger \hat{a}_l\right], \tag{3}$$

where $\hat{a}_l$ and $\hat{a}_l^\dagger$ denote annihilation and creation operators (bosonic or fermionic) at site l, respectively, t_α is the hopping term to the αth neighbor, and V_l models a local scalar potential at site l. Then, the helix geometry will make it necessary to take into account hopping terms with $\alpha > 1$, i.e., beyond nearest neighbor in index. This naturally generalizes the idea of planar zigzag lattices in which the second-neighbor hopping can be of the same order of magnitude as the nearest-neighbor hopping to the three-dimensional space, opening a way to make even more long-range hopping terms sizable. Crucially, we assume that the translational invariance of the model is preserved in the sense that the hopping amplitudes depend on index difference only. This is ensured if the full lattice potential landscape is invariant under the screw operation that for every l maps $\vec{r}_l$ to $\vec{r}_{l+1}$. We take the atoms to be effectively noninteracting here, a requirement that can experimentally be realized for many species by means of Feshbach resonance techniques [44]. In the above, we have simply assumed the existence of a Hubbard Hamiltonian as in Eq. (3). In other words, it is assumed that the three-dimensional potential landscape that constitutes the potential wells is such that Wannier-type modes localized at each lattice site exist and that in the regime considered it is sufficient to restrict to one such mode per site. While the existence and construction of localized Wannier modes for one-dimensional (1D) lattices with the usual discrete translation symmetry is well known, this is much less the case for a system with a basic symmetry under discrete screw operations, such as the helix lattice. Recently, it has been shown on abstract grounds that localized Wannier functions still exist for the latter type of problem, and a tight-binding Hamiltonian as in Eq. (3) has been justified [45].

In this work, we do not aim at constructing the Wannier states and calculating the Hubbard parameters from first principles. For a rough idea of the scaling of the hopping amplitudes t_α, we resort to the result of [46] where the hoppings in a lattice with the usual discrete translational symmetry are shown to decay exponentially with the Euclidean intersite distance, up to a polynomial prefactor. Let us assume, solely for the purpose of illustration, that this scaling also applies in the helix lattice landscape, say $t_n \sim \exp(-2d_n)$. This quantity is shown in Fig. 1(b), normalized to its value at $n = 1$. Clearly, there are several values whose order of magnitude is comparable to the $n = 1$ contribution. For the chosen geometry parameters, the dominant hoppings will be t_1 (to the nearest sites along the winding) and t_4 (to the nearest sites on the adjacent windings), with a strong decay beyond t_5. We emphasize that the actual helix hopping parameters will

depend on the detailed shape of the lattice potential, the heights of the potential barriers along and between the windings, etc., and finding them would require a band-structure calculation for the specific potential taking into account the screw symmetry. Since this may be a hard task, in the following we also suggest a way to experimentally extract the parameters from the Bloch dynamics of the system under a constant external force along the z axis, shown as dotted line in Fig. 1(c). Note that the helix geometry is such that for a potential linear in z, $V(\vec{r}) = F_0 z$, the values at the lattice sites scale linearly with the index, i.e., $V(\vec{r}_l) = F_0 b\varphi_0 l$.

Finally, we remark that arguably the proposals presently available suggest that a double-helix potential for cold atoms may be easier to realize experimentally than the single-helix strand we assume here. We can still restrict to the simple single-strand scenario since a noninteracting double-helix model with hoppings along and between the strands can be reduced to two decoupled copies of the single-strand model, as shown in Appendix A.

III. EQUATION OF MOTION AND FORCE-FREE LIMIT

In the following, we give a detailed analysis of the single-particle dynamics governed by the Hamiltonian (3). Expanding the state at time τ as $|\Psi\rangle_\tau = \sum_l \Psi_l(\tau)\hat{a}_l^\dagger|\emptyset\rangle$ where the Ψ_l are complex coefficients and $|\emptyset\rangle$ denotes the vacuum state, the Schrödinger equation for $|\Psi\rangle_\tau$ yields an equation of motion for the coefficients which in dimensionless form reads as

$$i\,\partial_\tau \Psi_l(\tau) = -\sum_{\alpha=1}^{A} t_\alpha \left[\Psi_{l+\alpha}(\tau) + \Psi_{l-\alpha}(\tau)\right] + Fl\Psi_l(\tau). \quad (4)$$

This result for a single particle is obtained both for bosonic and fermionic ladder operators. For an ensemble of many bosons, the same equation arises when approaching the noninteracting limit from the mean field (Gross-Pitaevskii) regime [47]. We have specified here the potential term V_l to be linear in l, modeling a constant force along the z axis in the helix example. For technical reasons, we take the number of nonzero hopping terms to be finite in the following, but the cutoff A can be arbitrarily large. We emphasize that while the helix lattice for ultracold atoms motivates our study of long-range hopping terms, the following considerations are based solely on Eq. (4) and apply in any context in which this equation arises.

As a first step, we establish some results on the discrete Schrödinger equation (4) in the force-free limit. As usual, stationary solutions are obtained by factorizing $\Psi_l(\tau) = \psi_l \exp(-iE\tau)$. It is straightforward to see that in the absence of an external force $F = 0$, Eq. (4) admits stationary plane-wave solutions of the form $\psi_l \propto \exp(ikl)$. This is a direct consequence of the translational invariance of the model. The corresponding dispersion relation of the infinitely extended lattice model is given by

$$E(k) = -2\sum_{\alpha=1}^{A} t_\alpha \cos(k\alpha), \quad -\pi < k \leqslant \pi. \quad (5)$$

It is apparent from Eq. (5) that the presence of long-range hopping terms leads to the emergence of the corresponding higher harmonics of k in the dispersion relation. Depending on the relative values of the t_α, this can dramatically alter the shape of the $E(k)$ curve, inducing for instance additional maxima and minima or causing a shift of the band edges to different values of k. An example of this is shown in Fig. 2, where for definiteness we have used the values displayed in Fig. 1(b) for the t_α (with a cutoff at $A = 8$).

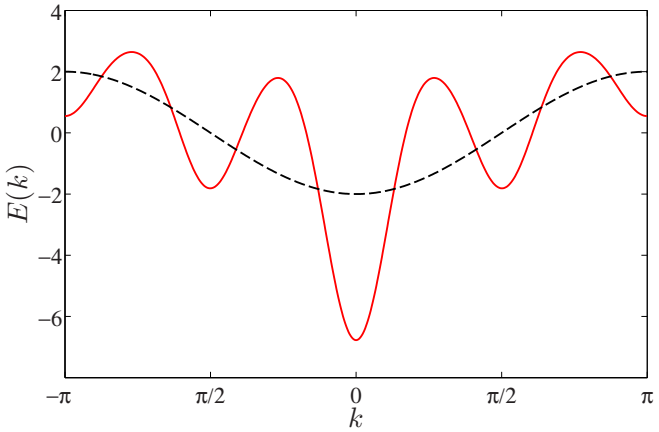

FIG. 2. (Color online) Band structure given by Eq. (5) for a model with long-range hoppings as in Fig. 1(b) (red solid line) and of a nearest-neighbor model with only $t_1 = 1$ (black dashed line).

For the zigzag limiting case of only t_1 and t_2 nonvanishing, this type of deformation of the band structure has been discussed in detail in [22], pointing out also a number of consequences for the localized solutions of the corresponding discrete nonlinear Schrödinger model. A general property to be read off from Eq. (5) is that the global minimum of E is assumed at $k = 0$ as long as all $t_\alpha \geqslant 0$. That is, if the signs of all hopping parameters are such that they energetically favor the linked sites to be in phase, the ground state is simply given by the zero quasimomentum state. If, in contrast, there are hopping terms with $t_\alpha < 0$ present in the system, this favors a phase difference of π between sites of distance α. Depending on the detailed values of the t_α, this may cause frustration and thus lead to a nontrivial ground state. Again restricting to the zigzag limit, phase diagrams of interacting models in this interesting frustrated regime have been studied recently in [48,49].

IV. WANNIER-STARK STATES AND PROPAGATOR

As soon as the force parameter $F \neq 0$, plane waves no longer solve Eq. (4). Instead, there is now a complete set of localized modes, the Wannier-Stark states [29,50,51]. Their construction for the discrete Schrödinger model by transforming to momentum space, as detailed for example in [52], can be extended in a straightforward way to take into account the presence of long-range hoppings. We find the Wannier-Stark modes to be given by

$$\chi_l^{(w)} = \frac{1}{2\pi}\int_0^{2\pi} dk \exp\left[i(l-w)k - i\sum_{\alpha=1}^{A}\frac{2t_\alpha}{\alpha F}\sin(k\alpha)\right]. \quad (6)$$

Each Wannier-Stark state is labeled by an integer quantum number $w \in \mathbb{Z}$, and its energy eigenvalue is given by $E_w = wF$. This equidistant spectrum, the so-called Wannier-Stark ladder, is insensitive to the presence of long-range hoppings. The fact that all energy eigenvalues are harmonics of the fundamental frequency F immediately implies that the dynamics of any initial state is periodic with period $T_B = 2\pi/F$. This includes the famous Bloch oscillations of a wave packet localized in momentum space, but is also true for any other initial condition.

To proceed, we use the Jacobi-Anger expansion [53]

$$e^{-iz\sin\phi} = \sum_{n=-\infty}^{\infty} J_n(z)e^{-in\phi}, \tag{7}$$

where J_n denotes the nth Bessel function of the first kind. Then, the integral in Eq. (6) can be evaluated to

$$\chi_l^{(w)} = \sum_{n_1,\ldots,n_A} \delta_{\sum_{\alpha=1}^{A}\alpha n_\alpha, l-w} \prod_{\alpha=1}^{A} J_{n_\alpha}\left(\frac{2t_\alpha}{\alpha F}\right), \tag{8}$$

where all indices n_α are summed over $\mathbb{Z}$. In the limit of only nearest-neighbor hopping, $t_\alpha = 0$ for $\alpha \geqslant 2$, we have $J_{n_\alpha}(\frac{2t_\alpha}{\alpha F}) = \delta_{n_\alpha,0}$ for $\alpha \geqslant 2$, such that $\chi_l^{(w)} = J_{l-w}(\frac{2t_1}{F})$ in this limit, reproducing the result of [29].

Using basic properties of the Bessel functions (see also below), we can immediately establish some properties of the Wannier-Stark states from Eq. (8). First, the Wannier-Stark mode of quantum number w is centered at site w since $\sum_l l|\chi_l^{(w)}|^2 = w$. Second, for increasing values of F the mode becomes more and more localized since

$$\sum_l l^2|\chi_l^{(w)}|^2 - w^2 = \frac{2}{F^2}\sum_{\alpha=1}^{A} t_\alpha^2. \tag{9}$$

We see here how the presence of long-range hopping terms favors a delocalization of the Wannier-Stark states. Single-site localization sets in when the force is so strong that $F^2 \gg \sum_\alpha t_\alpha^2$.

When restricting to next-neighbor hopping, the Wannier-Stark mode has the symmetry $\chi_{w-l}^{(w)} = (-1)^l\chi_{w+l}^{(w)}$ which ensures that the density is symmetric around the central site w. This symmetry property is lost if additional hoppings are taken into account. Instead, the stationary localized modes described by Eq. (8) generally exhibit intricate asymmetric density distributions around the central site. This is illustrated in Fig. 3, which also shows the localization that increases with F.

Since the Hamiltonian is diagonal in the Wannier-Stark basis, we can immediately write the matrix elements of the propagator

$$U_{l,l'}(\tau) = \sum_{w\in\mathbb{Z}} \chi_l^{(w)}\left(\chi_{l'}^{(w)}\right)^* e^{-iwF\tau}. \tag{10}$$

Inserting the expansion of the Wannier-Stark modes given in Eq. (8) and repeatedly making use of the identity [53]

$$\sum_{n=-\infty}^{\infty} J_n(z)J_{n+j}(z)e^{in\phi} = J_j\left(2z\sin\frac{\phi}{2}\right)i^j e^{-ij\phi/2}, \tag{11}$$

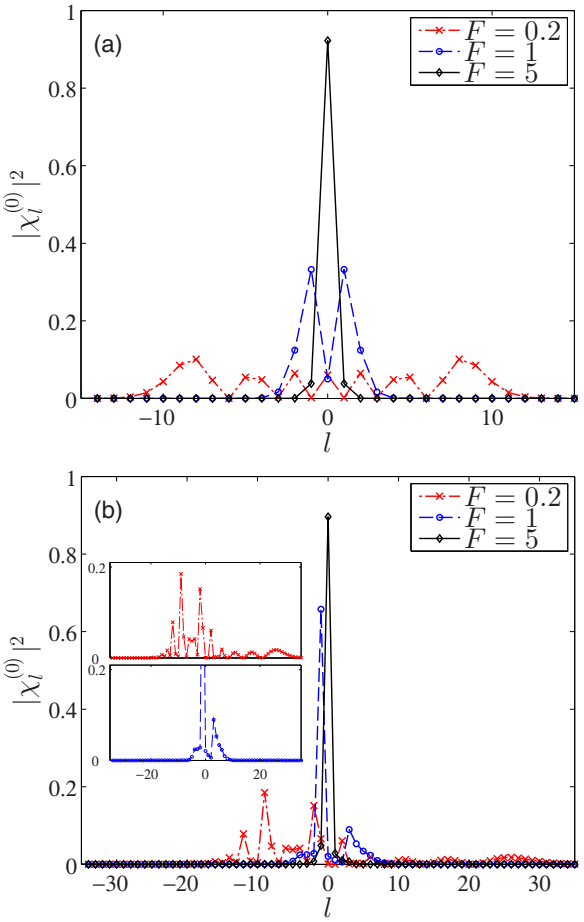

FIG. 3. (Color online) Density profiles of Wannier-Stark states centered at $l = 0$ at different values of F as listed in the legend for (a) a nearest-neighbor model with only $t_1 = 1$, (b) a model with long-range hoppings $t_1 = t_2 = t_3 = 1$, where the insets show a zoom of the low-density region for the less localized states at smaller F.

this is evaluated to be

$$U_{l,l'}(\tau) = i^{l-l'}e^{-i\frac{F\tau}{2}(l+l')} \times \sum_{n_2,\ldots,n_A} J_{l-l'-\sum_{\alpha=2}^{A}\alpha n_\alpha}\left(\frac{4t_1}{F}\sin\frac{F\tau}{2}\right) \times \prod_{\alpha=2}^{A} i^{-n_\alpha(\alpha-1)}J_{n_\alpha}\left(\frac{4t_\alpha}{\alpha F}\sin\frac{F\tau\alpha}{2}\right). \tag{12}$$

Again, let us discuss some limiting cases. If all hoppings are turned off, the propagator collapses to $U_{l,l'}(\tau) = \delta_{l,l'}e^{-iFl\tau}$, corresponding to decoupled sites whose phases evolve with the respective local potential. When we restrict ourselves to the nearest-neighbor hopping term, we arrive at the result of [29] (see also [34,52,54,55]). Finally, taking the limit of $F \to 0$ and noting that $\lim_{\epsilon\to 0}\frac{\sin\epsilon}{\epsilon} = 1$, we recover the propagator of a force-free lattice with arbitrary long-range hoppings recently obtained in [27].

V. BLOCH DYNAMICS OF WAVE PACKETS

Having derived the closed expression for the propagator, we are now in the position to study the dynamics of an arbitrary initial wave function. Let us start by discussing the simple case of an initial single-site excitation $\Psi_l(\tau=0)=\delta_{l,l_0}$. Then, the wave function at time τ is obtained using the propagator from Eq. (12) as

$$\Psi_l(\tau)=\sum_{l'}U_{l,l'}(\tau)\Psi_{l'}(\tau=0)=U_{l,l_0}(\tau). \tag{13}$$

From the properties of the Bessel function, one finds that even in the presence of long-range hoppings the propagator has the symmetry $|U_{l_0-l,l_0}(\tau)|=|U_{l_0+l,l_0}(\tau)|$ for any l_0,l and any τ. Thus, during the time evolution following the initial single-site excitation, the density will remain left-right symmetric around the central site l_0. In particular, the center of mass remains at rest at l_0. The width, however, can change as a function of time, and from the equidistant spacing of the Wannier-Stark spectrum it is clear that the dynamics of the width has to be oscillatory with period $T_B=2\pi/F$. This Bloch breathing behavior is well known for nearest-neighbor models.

On the other hand, if the initial excitation is not restricted to a single site, but rather a wave packet that is sufficiently delocalized in position space to be considered localized in k space, then this wave packet will perform Bloch oscillations under the influence of the external force. The temporal periodicity is the same as for the Bloch breathings, but now the center of mass of the wave packet performs oscillations while its shape is essentially unchanged. In most cases, the theoretical description of these Bloch oscillations is based on a semiclassical argument explicated below.

In spite of the qualitative differences between Bloch breathing and Bloch oscillations, these dynamics are two sides of the same coin and are both captured by the propagator in Eq. (12). In the following, our aim is twofold: First, we discuss the crossover from Bloch breathing to Bloch oscillations by considering an initial Gaussian wave packet of variable width. This is done for arbitrary long-range hoppings, and in a second step we work out the limiting cases of pure Bloch breathing and pure Bloch oscillations for lattices with long-range hoppings and provide quantitative estimates for which parameter values of the model these limits apply.

To explore the crossover region, we consider as the initial state a site-centered Gaussian wave packet defined by

$$\Psi_l(\tau=0)=\mathcal{N}e^{-l^2/(2\sigma)},\qquad \sigma>0. \tag{14}$$

More general initial conditions are discussed in Appendix B. Without loss of generality, we take the wave packet to be centered at site 0 initially. In the limit of small σ, Eq. (14) describes essentially a single-site excitation that, as seen above, will perform Bloch breathing. In contrast, if σ is large we expect Bloch oscillations of the wave packet's center of mass, with no notable deformation.

First of all, we find that the normalization constant $\mathcal{N}$ is evaluated to be $1/\mathcal{N}^2=\sum_l e^{-l^2/\sigma}=\vartheta_3(0,e^{-1/\sigma})$, where ϑ_3 denotes the Jacobi theta function of the third kind [56] defined as

$$\vartheta_3(u,q)=1+2\sum_{n=1}^{\infty}q^{n^2}\cos 2nu,\qquad |q|<1 \tag{15}$$

which will also become important below. With this, we can evaluate the two key quantities to characterize and distinguish Bloch breathing and Bloch oscillations, namely, the first two moments of the position operator $\langle X\rangle_\tau=\sum_l l|\Psi_l(\tau)|^2$ and $\langle X^2\rangle_\tau=\sum_l l^2|\Psi_l(\tau)|^2$. These quantities can be obtained through a lengthy but direct calculation, making repeated use of the Bessel function orthogonality and recursion identities [53] [the former being a special case of Eq. (11)]

$$\sum_l J_l(z)J_{l+j}(z)=\delta_{j,0}, \tag{16a}$$

$$lJ_l(z)=\frac{z}{2}[J_{l-1}(z)+J_{l+1}(z)]. \tag{16b}$$

Defining the auxiliary function $g(\alpha,\sigma)$ for $\alpha\in\mathbb{N}$ as

$$g(\alpha,\sigma)=\sum_l\Psi_l(\tau=0)\Psi_{l+\alpha}(\tau=0)$$

$$=e^{-\alpha^2/(4\sigma)}\,\frac{\vartheta_3\left(\alpha\frac{\pi}{2},e^{-\sigma\pi^2}\right)}{\vartheta_3(0,e^{-\sigma\pi^2})}, \tag{17}$$

we finally obtain compact expressions for the first two moments of the position operator:

$$\langle X\rangle_\tau=-\sum_{\alpha=1}^{A}\frac{4t_\alpha}{F}g(\alpha,\sigma)\sin^2\frac{\alpha F\tau}{2}, \tag{18}$$

$$\begin{aligned}\langle X^2\rangle_\tau=\langle X^2\rangle_{\tau=0}&+\sum_{\alpha=1}^{A}\frac{8t_\alpha^2}{F^2}\sin^2\frac{\alpha F\tau}{2}\\&\times[1-g(2\alpha,\sigma)\cos(\alpha F\tau)]\\&+\sum_{\alpha>\beta}\frac{16t_\alpha t_\beta}{F^2}\sin\frac{\alpha F\tau}{2}\sin\frac{\beta F\tau}{2}\\&\times\left[g(\alpha-\beta,\sigma)\cos\frac{(\alpha-\beta)F\tau}{2}\right.\\&\left.-g(\alpha+\beta,\sigma)\cos\frac{(\alpha+\beta)F\tau}{2}\right].\end{aligned} \tag{19}$$

Details on the derivation of Eqs. (18) and (19) are provided in Appendix B, where also the corresponding generalizations to arbitrary initial conditions are given. From these equations, it is immediately seen that the presence of long-range hoppings introduces higher harmonics of the fundamental Bloch frequency F in the time evolution of $\langle X\rangle_\tau$ and $\langle X^2\rangle_\tau$. Intuitively, these harmonics are expected to show up since the potential difference between two sites of index difference α is proportional to α in our model, thus, the effective Bloch frequency when considering hopping only to the αth neighbor is given by the harmonic αF. The second observation to be made is that g acts as a crossover function, interpolating between Bloch breathing for small σ and Bloch oscillations for large σ. This is reflected by the limits

$$g(\alpha,\sigma)\longrightarrow\begin{cases}0, & \sigma\to 0\\ 1, & \sigma\to\infty\end{cases} \tag{20}$$

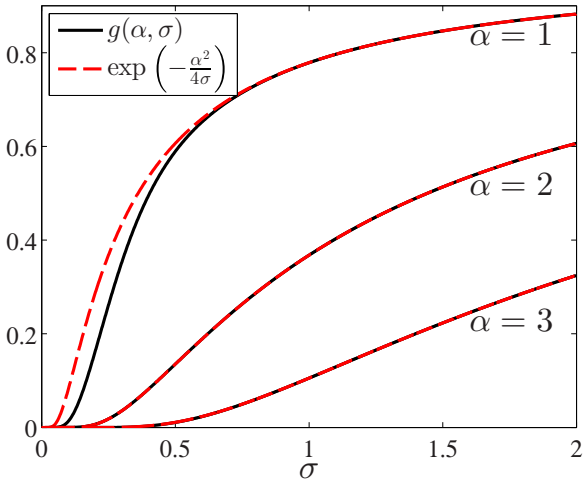

FIG. 4. (Color online) Full crossover function g, compared to the plain exponential factor, as a function of σ for various values of α. In the limit of large σ, all curves tend to 1.

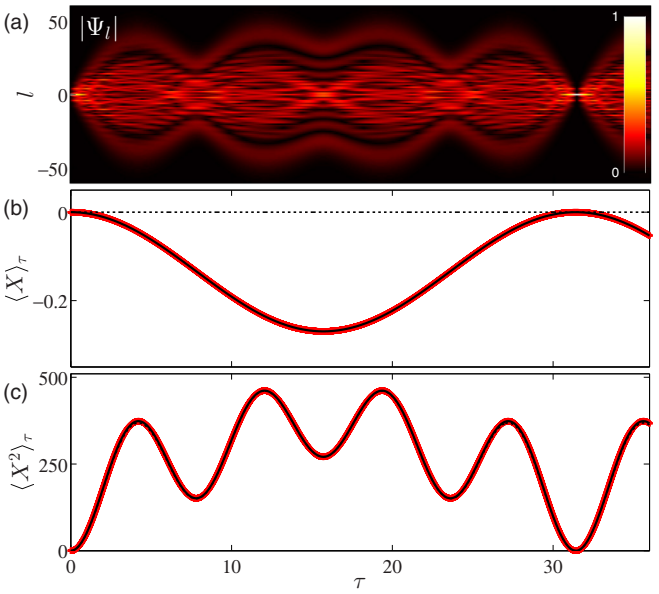

FIG. 5. (Color online) Multifrequency Bloch breathing oscillation of a narrow Gaussian wave packet with $\sigma = 0.1$ at $F = 0.2$, hopping parameters as in Fig. 1(b). (a) Absolute value of Ψ_l as a function of time τ and site index l. (b), (c) First two moments of the position operator: numerical values (black lines), analytical result of Eqs. (18) and (19) (red markers) and approximations of Eqs. (22) and (23) (dashed black lines).

holding for any nonzero α. We furthermore see that the overall shape of g is strongly determined by the exponential prefactor. Distinguishing the case of the integer argument α being even or odd, one finds

$$g(\alpha,\sigma) = \begin{cases} e^{-\alpha^2/(4\sigma)}, & \alpha \text{ even} \\ e^{-\alpha^2/(4\sigma)} \dfrac{\vartheta_3\left(\frac{\pi}{2}, e^{-\sigma\pi^2}\right)}{\vartheta_3\left(0, e^{-\sigma\pi^2}\right)}, & \alpha \text{ odd.} \end{cases} \tag{21}$$

The correction factor $\vartheta_3(\pi/2, e^{-\sigma\pi^2})/\vartheta_3(0, e^{-\sigma\pi^2})$ occurring for α odd here is close to unity for not too small values of σ since $\exp(-\sigma\pi^2)$ quickly goes to zero with increasing σ. Thus, the second argument of the Jacobi theta functions quickly decays to zero and both theta functions approach unity. On the other hand, for small σ the correction factor goes to zero, so the relative deviation between g and the plain exponential $\exp[-\alpha^2/(4\sigma)]$ becomes large. The absolute error, however, is small still, since the value of the exponential itself approaches zero in this limit (the larger α, the faster). Figure 4 shows the full $g(\alpha,\sigma)$ for $\alpha = 1,2,3$ and in comparison also the exponential factor $\exp[-\alpha^2/(4\sigma)]$. For large σ, where it eventually approaches unity, g is fully dominated by the exponential. This also implies that the convergence to 1 is slower the larger α, a trend that is clearly observed when going from $\alpha = 1$ to 3 already. For small σ, a notable deviation between g and the exponential can be seen for $\alpha = 1$. For $\alpha = 2$ (and any other even α) the agreement is exact. For $\alpha = 3$, the absolute deviations due to the Jacobi theta function correction factor are already so small that they cannot be identified on the scale of this figure.

Let us now discuss separately the two limiting cases of small and large width of the initial wave packet, respectively. For $\sigma \to 0$, so all occurrences of $g \to 0$ in Eqs. (18) and (19), we find

$$\langle X\rangle_\tau = 0, \tag{22}$$

$$\langle X^2\rangle_\tau = \sum_\alpha \frac{4t_\alpha^2}{F^2}\left[1 - \cos(\alpha F\tau)\right]. \tag{23}$$

We see that in this limit the center of mass is at rest while the wave packet width performs oscillations. This is characteristic of a pure Bloch breathing dynamics, where the long-range hopping terms contribute oscillations at higher harmonics of the Bloch frequency F. This includes the two-frequency Bloch breathing recently observed in zigzag lattices with nonvanishing t_1 and t_2 [26]. Figure 5 shows the time evolution of a narrow Gaussian wave packet obtained by directly integrating the discrete Schrödinger equation (4). The moments of the position operator are evaluated numerically (red markers) and as a check compared to the analytical expressions of Eqs. (18) and (19) (black lines), showing agreement. The approximate predictions of Eqs. (22) and (23) are shown as dashed lines. It is clearly observed that this situation is very close to the pure Bloch breathing limit, with the center of mass being almost at rest. For the width oscillation, the deviation from Eq. (23) is almost indiscernible on the scale of this figure. The Bloch period is given by $T_B = 10\pi$ for the chosen parameters. After this time, a full refocusing of the localized excitation is observed.

Again, we note that Eq. (23) contains special cases that have been reported before. The corresponding expression for next-neighbor hopping only is given in [34]. In the force-free limit, the recent result of [28] for the ballistic spreading of a single-site excitation in a lattice with long-range hoppings is recovered, i.e., $\langle X^2\rangle_\tau \to 2\tau^2 \sum_\alpha \alpha^2 t_\alpha^2$ for $F \to 0$. Conversely, in the work [30] that is primarily concerned with ac driven

nearest-neighbor lattice systems, an extension to long-range hoppings is sketched which when worked out [57] reduces to Eq. (23) in the static limit.

In the opposite limit of $\sigma \to \infty$, all occurrences of $g \to 1$. Then, Eqs. (22) and (23) give

$$\langle X\rangle_\tau = -\sum_\alpha \frac{2t_\alpha}{F}[1-\cos(\alpha F\tau)], \tag{24}$$

$$\langle X^2\rangle_\tau - \langle X\rangle_\tau^2 = \langle X^2\rangle_{\tau=0} = \frac{\sigma}{2}. \tag{25}$$

These trajectories describe a multifrequency Bloch oscillation of the wave packet as a whole, as can be inferred from the time-independent variance of X. For two nonvanishing hopping terms, such a two-frequency oscillation has been predicted and observed in [25,26].

We show now that Eq. (24) agrees with the result found from the simple semiclassical argument usually invoked to discuss Bloch oscillations: If the initial wave packet is sufficiently delocalized in position space, and thus localized in quasimomentum space, one can obtain the time evolution of its quasimomentum from the acceleration theorem [58,59] as $k(\tau) = -F\tau$. The velocity $v(\tau)$ of the wave packet is then given by the group velocity evaluated at $k(\tau)$, i.e.,

$$v(\tau) = \left.\frac{dE}{dk}\right|_{k=-F\tau} = -2\sum_\alpha \alpha t_\alpha \sin(\alpha F\tau), \tag{26}$$

and integrating this equation gives the center-of-mass motion $\langle X\rangle_\tau$ found in Eq. (24). This way of reasoning directly links the Bloch oscillation trajectory to the band structure. Thus, the additional maxima and minima of $E(k)$ that exist due to the presence of long-range hoppings immediately cause additional reversal points of the wave-packet dynamics within one Bloch period. In Fig. 6, we present a numerical simulation of a multifrequency Bloch oscillation, verifying again the validity of Eqs. (18) and (19) against the direct solution of the equation of motion (4). Indeed, we see that for this comparably large initial width we approach a regime in which the trajectory closely follows the predictions of Eqs. (24) and (25) shown as dashed lines, although there are still deviations in both $\langle X\rangle_\tau$ and $\langle X^2\rangle_\tau$. These deviations are particularly visible when calculating the variance that deviates still quite strongly from the constant value $\sigma/2$. We find that going to larger values of σ, these features are further diminished and the semiclassical equations become more and more exact.

Equations (23) and (24) allow us to calculate the Bloch breathing and oscillation trajectories given the model parameters t_α and F. Conversely, measuring these trajectories and Fourier transforming them provides a way to extract the hopping parameters t_α and the force F from the time evolution data. The frequency spectra will have peaks at the harmonics αF with amplitudes determined by the ratios t_α/F. We remark that since sparse frequency spectra are expected here, this problem should be an ideal candidate for so-called compressed sensing techniques which admit a reliable reconstruction of the spectrum even from imperfect time signals (see [60] for an introduction and [61] for a recent application in the context of molecular dynamics).

So far, we have focused on the limiting cases of ideal Bloch breathing on the one hand and ideal Bloch oscillations

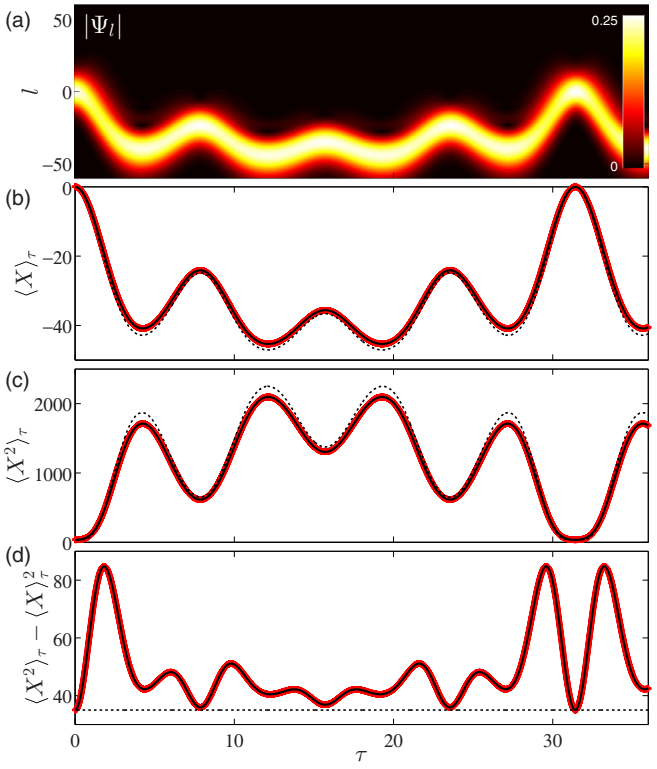

FIG. 6. (Color online) Multifrequency Bloch oscillation of a wide Gaussian wave packet with $\sigma = 70$ at $F = 0.2$, hopping parameters as in Fig. 1(b). (a) Absolute value of Ψ_l as a function of time τ and site index l. (b)–(d) First two moments and variance of the position operator: numerical values (black lines), analytical result of Eqs. (18) and (19) (red markers) and approximations of Eqs. (24) and (25) (dashed black lines).

on the other hand. Equations (18) and (19) hold for the full crossover between these two limits, however, and from a study of the function g we can also estimate that there is a large intermediate regime that is neither characterized by a pure breathing nor by a pure center-of-mass oscillation. To reach the limit of Bloch breathing with $\langle X\rangle_\tau \approx 0$, from Eq. (18) we can read off the necessary condition that $g(\alpha,\sigma) \approx 0$ for all α for which t_α is non-negligible. Since g approaches zero faster for $\sigma \to 0$ the larger α, this condition is most restrictive for $\alpha = 1$. Consequently, in a system with non-negligible next-neighbor hopping we can expect to reach the pure Bloch breathing limit when $g(1,\sigma) \approx 0$, which is the case for $\sigma \lesssim 0.1$ (see Fig. 4). At $\sigma = 0.1$, the initial probability to find the particle away from the central site 0 is already of the order of 10^{-4}, so to observe pure Bloch breathing one indeed needs an essentially pure single-site excitation. Any sizable excitation of neighboring sites will induce deviations from $\langle X\rangle_\tau = 0$ and cause center-of-mass oscillations according to Eq. (18). In Fig. 5, it is clearly observed that even at $\sigma = 0.1$, the center-of-mass motion is not completely suppressed.

Turning to the pure Bloch oscillation limit of $\sigma \to \infty$, from Eq. (18) we can infer the condition $g(\alpha,\sigma) \approx 1$ for all α for which the hopping term t_α is non-negligible. We have seen above that the behavior of g at large σ is entirely determined by the exponential $\exp[-\alpha^2/(4\sigma)] \sim 1 - \alpha^2/(4\sigma)$

for large σ. Thus, for the center of mass to be described by the semiclassical Bloch trajectory, the condition $4\sigma \gg \alpha^2$ needs to be satisfied for any α with sizable hopping t_α. From the above semiclassical discussion it is to be expected that the hopping terms of largest α give the strictest condition here: The considerations leading to Eq. (26) rely on a linearization of the dispersion relation E around the central momentum of the wave packet. Higher-order hoppings lead to short length scale oscillations in the $E(k)$ curve as seen in Fig. 2, deteriorating the linearization approximation and thus enforcing a stronger localization of the wave packet in k space for the analysis to apply, which in turn demands a larger spread in direct space. Even if $4\sigma \gg \alpha^2$ is fulfilled for any α with non-negligible t_α, it is not directly ensured that the variance also follows the semiclassical expectation $\langle X^2\rangle_\tau - \langle X\rangle_\tau^2 = \langle X^2\rangle_{\tau=0}$. For this to hold, we also need the $g \approx 1$ limit to hold for all terms in Eq. (19). In particular, this poses the necessary condition that also $g(2\alpha,\sigma) \approx 1$ for all α with non-negligible t_α, implying the stricter condition $\sigma \gg \alpha^2$. In line with this argument, a close inspection of Fig. 6 indeed shows that the relative deviations of the true trajectory from the semiclassical expectation are larger for $\langle X^2\rangle_\tau$ and the variance than for $\langle X\rangle_\tau$.

Moving away from either of the two limits, the dynamics performed by a Gaussian wave packet of intermediate width consists of nontrivial oscillations both in the center of mass and the variance. An example illustrating this is shown in Fig. 7. The initial stage of the dynamics is characterized by a widening of the wave packet into both directions of the lattice, but in an asymmetric way, with a larger fraction moving to $l < 0$ and following a Bloch oscillation-type trajectory there. After the Bloch period, the wave packet is fully reconstructed.

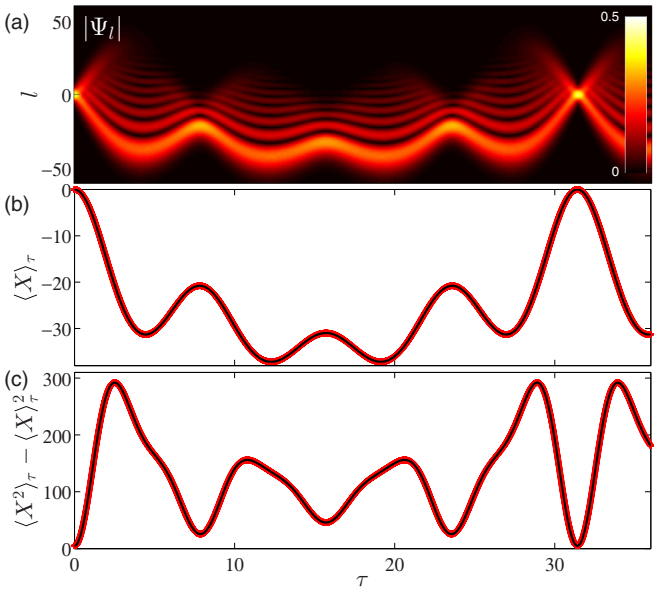

FIG. 7. (Color online) Intermediate case with nontrivial dynamics both in center of mass and width for an initial Gaussian wave packet with $\sigma = 10$ at $F = 0.2$, hopping parameters as in Fig. 1(b). (a) Absolute value of Ψ_l as a function of time τ and site index l. (b), (c) Expectation value and variance of the position operator: numerical values (black lines) and analytical result of Eqs. (18) and (19) (red markers).

VI. BRIEF SUMMARY AND PERSPECTIVES

We have investigated a translationally invariant discrete Schrödinger equation with arbitrary long-range hopping terms. The study of this equation was motivated by a proposal for a helix lattice for ultracold atoms, extending the idea of a planar zigzag lattice to three spatial dimensions. With such a lattice setup it will be possible to tune the long-range hoppings of a cold-atom Hubbard model through the helix geometry parameters. We have discussed the plane-wave solutions and dispersion relation of the force-free model and then turned to the influence of an external force. Closed expressions for the Wannier-Stark states and the propagator were constructed in terms of Bessel functions. Finally, we analyzed the Bloch dynamics of a Gaussian wave packet of arbitrary width. Our findings quantitatively describe the anharmonic Bloch dynamics observed in recent experiments [26] and are applicable in the full crossover regime between Bloch breathing of single-site excitations and Bloch oscillations of wide wave packets.

A promising framework [62] for the experimental realization of cold-atom helix lattices is provided by nanofiber-based optical trapping techniques as recently demonstrated [63,64]. In these experiments, cold atoms are trapped in the two-color evanescent light field above the surface of a tapered optical nanofiber. This setup is highly versatile, allowing for combinations of running or standing light waves of different frequencies and polarizations, and also for local variations of the fiber radius. It was shown that using circularly polarized light results in a continuous double-helix-shaped potential of tunable parameters [39], while parallel linear polarization gives rise to a sequence of linearly arranged potential wells of equidistant spacing [63]. These two limiting cases can be continuously transformed into each other using elliptically polarized light of varying ellipticity. In the intermediate regime, this will induce the desired lattice-type modulation of the double-helix curve. In its basic implementation, this scheme will produce two potential wells per winding for each of the helix strands, but the number can be increased by quickly switching the orientation of the polarization axes, resulting in a time-averaged potential for the atoms.

In this work, we have restricted to the single-particle dynamics of the helix lattice model. Combining the long-range hoppings with a local onsite interaction term will open a variety of directions for future studies. Within the bosonic mean field framework, one is led to a discrete nonlinear Schrödinger equation with long-range hoppings, reducing to Eq. (4) in the noninteracting limit. Previous studies have shown that the presence of beyond nearest-neighbor hoppings in such a model may drastically alter the properties of its localized excitations (see, e.g. [18,22,24]), but these considerations have been restricted to second-neighbor hopping only or to hoppings decreasing monotonically with the index difference. Going beyond the mean field approximation, it has been argued that long-range hoppings in a one-dimensional model can effectively mimic higher dimensionalities (see [65] for a recent example). A helix lattice setup may thus serve to experimentally address the crossover between a purely one-dimensional system (by suppressing interwinding tunneling) and a system with two-dimensional characteristics

(by using many sites per winding and sizable intrawinding and interwinding tunnelings). On the theoretical side, such a dimensional crossover is subject to active research even for cubic lattices [66]. Furthermore, the existence of frustration effects for negative hopping parameters has already been mentioned in Sec. III, pointing to interesting ground-state features in this regime. Notably, the well-known mapping from hard-core bosons to noninteracting fermions often employed for the standard Hubbard model breaks down in the presence of long-range hoppings (see, e.g., [67]). Finally, we mention the additional possibility of introducing long-range interactions into the helix lattice framework, for instance of the dipolar or Coulomb type. Recently, such systems with the particle dynamics being constrained to low-dimensional structures but the interaction exploring the surrounding space have received considerable attention [40,68–71].

ACKNOWLEDGMENTS

We thank A. Rauschenbeutel and P. G. Kevrekidis for insightful discussions. J.S. gratefully acknowledges support from the Studienstiftung des deutschen Volkes.

APPENDIX A: DOUBLE-HELIX LATTICE MODEL AND ITS REDUCTION

The recent proposals [38,39] for the experimental creation of helical waveguides for ultracold atoms result in double-helix structures, rather than in a single-strand helix as discussed here. In this appendix, we introduce a double-helix lattice system and show that its single-particle dynamics can be reduced to that of the single-strand model.

Adopting notation from the main text, we label the two strands of the double helix by (I) and (II) and take them to be parametrized by $\vec{r}^{(\mathrm{I})}(\varphi) = (R\cos\varphi, R\sin\varphi, b\varphi)$ and $\vec{r}^{(\mathrm{II})}(\varphi) = (-R\cos\varphi, -R\sin\varphi, b\varphi)$, respectively. We assume a symmetric geometry in which the potential wells forming the lattice sites are spaced equidistantly (in terms of arc length) on the two strands, with the same site-to-site distance for both strands. Furthermore, we take the geometry to be chosen such that lattice sites on the different strands are located at identical z coordinates. Summarizing, we assume site positions

$$\vec{r}_l^{(\mathrm{I})} = (R\cos(l\varphi_0), R\sin(l\varphi_0), b\varphi_0 l),$$
$$\vec{r}_l^{(\mathrm{II})} = (-R\cos(l\varphi_0), -R\sin(l\varphi_0), b\varphi_0 l)$$

for some fixed φ_0. This makes sure that the Euclidean distances between a site and its nth neighbor on both the same strand and the opposite strand depend on the index difference only. With Hubbard parameters given by t_α ($\alpha \geqslant 0, t_0 = 0$) for hopping to the αth neighbor in index on the same strand and t'_α ($\alpha \geqslant 0$) for hopping to the αth neighbor in index on the opposite strand, considerations analogous to those in the main text give rise to two coupled discrete Schrödinger equations for the single-particle dynamics under a constant force along the z axis

$$i\partial_\tau \Psi_l^{(\mathrm{I})} = -\sum_\alpha \left[t_\alpha \left(\Psi_{l+\alpha}^{(\mathrm{I})} + \Psi_{l-\alpha}^{(\mathrm{I})} \right) + t'_\alpha \left(\Psi_{l+\alpha}^{(\mathrm{II})} + \Psi_{l-\alpha}^{(\mathrm{II})} \right) \right] + Fl\Psi_l^{(\mathrm{I})},$$
$$i\partial_\tau \Psi_l^{(\mathrm{II})} = -\sum_\alpha \left[t_\alpha \left(\Psi_{l+\alpha}^{(\mathrm{II})} + \Psi_{l-\alpha}^{(\mathrm{II})} \right) + t'_\alpha \left(\Psi_{l+\alpha}^{(\mathrm{I})} + \Psi_{l-\alpha}^{(\mathrm{I})} \right) \right] + Fl\Psi_l^{(\mathrm{II})}.$$

This system can be readily decoupled (cf. [16]) via the transformation $\Psi_l^{(\pm)} := (\Psi_l^{(\mathrm{I})} \pm \Psi_l^{(\mathrm{II})})/\sqrt{2}$, resulting in

$$i\partial_\tau \Psi_l^{(+)} = -\sum_{\alpha=0}^{\infty} (t_\alpha + t'_\alpha)\left(\Psi_{l+\alpha}^{(+)} + \Psi_{l-\alpha}^{(+)}\right) + Fl\Psi_l^{(+)}, \quad i\partial_\tau \Psi_l^{(-)} = -\sum_{\alpha=0}^{\infty} (t_\alpha - t'_\alpha)\left(\Psi_{l+\alpha}^{(-)} + \Psi_{l-\alpha}^{(-)}\right) + Fl\Psi_l^{(-)},$$

which is a set of two independent copies of the single-strand lattice model studied in this work. Thus, all our results can immediately be carried over to the noninteracting double-strand lattice. In particular, if the initial wave function is such that opposing sites on the two strands are equally populated and in phase, $\Psi_l^{(-)}$ will vanish for all times, and $\Psi_l^{(+)} = \sqrt{2}\Psi_l^{(\mathrm{I})} = \sqrt{2}\Psi_l^{(\mathrm{II})}$ will immediately be governed by a discrete Schrödinger equation as Eq. (4).

APPENDIX B: GENERAL EXPRESSIONS FOR THE FIRST TWO MOMENTS OF THE POSITION OPERATOR

In this Appendix, we extend the results of Sec. V by considering an arbitrary (normalized) initial wave function $\Psi_l(0)$. We derive closed expressions for the time dependence of the first two moments of the position operator in terms of this initial condition. The general result is then specialized to the one for the Gaussian wave packet as provided in Sec. V.

Using the explicit form of the propagator given in Eq. (12), we find for any power p of the position operator

$$\langle X^p \rangle_\tau = \sum_l l^p \Psi_l^*(\tau)\Psi_l(\tau) = \sum_{l,l',l''} l^p U_{l,l'}(\tau) U_{l,l''}^*(\tau)\Psi_{l'}(0)\Psi_{l''}^*(0)$$
$$= \sum_{l',l''} \Psi_{l'}(0)\Psi_{l''}^*(0) i^{l''-l'} e^{i\frac{F\tau}{2}(l''-l')} \sum_{\{n_\alpha, n'_\alpha\}_{\alpha=2}^A} i^{\sum_{\alpha=2}^A (\alpha-1)(n'_\alpha - n_\alpha)} \prod_{\alpha=2}^A [J_{n_\alpha}(\xi_\alpha) J_{n'_\alpha}(\xi_\alpha)] \sum_l l^p J_{l-l'-\sum_{\alpha=2}^A \alpha n_\alpha}(\xi_1) J_{l-l''-\sum_{\alpha=2}^A \alpha n'_\alpha}(\xi_1)$$

with the shorthand $\xi_\alpha = \frac{4t_\alpha}{\alpha F}\sin\frac{\alpha F\tau}{2}$. The strategy is now to employ the recursion and orthogonality relations of the Bessel functions provided in Eq. (16) to first evaluate the sum over l. We show this explicitly for $p=1$, where Eq. (16) yields

$$\sum_l l J_{l-l'-\sum_{\alpha=2}^A \alpha n_\alpha}(\xi_1) J_{l-l''-\sum_{\alpha=2}^A \alpha n'_\alpha}(\xi_1) = \left(l' + \sum_{\beta=2}^A \beta n_\beta\right)\delta_{l''-l',\sum_{\alpha=2}^A \alpha(n_\alpha - n'_\alpha)} + \frac{\xi_1}{2}\left(\delta_{l''-l',\sum_{\alpha=2}^A \alpha(n_\alpha-n'_\alpha)+1} + \delta_{l''-l',\sum_{\alpha=2}^A \alpha(n_\alpha-n'_\alpha)-1}\right).$$

Inserting this, evaluating the sum over l'' using the Kronecker symbols, and introducing the summation indices $m_\alpha = n_\alpha - n'_\alpha$, this results in

$$\begin{aligned}\langle X\rangle_\tau = &\sum_{l'}\sum_{\{n_\alpha,m_\alpha\}} \Psi_{l'}(0)\Psi^*_{l'+\sum_\alpha \alpha m_\alpha}(0) i^{\sum_\alpha m_\alpha} e^{i\frac{F\tau}{2}\sum_\alpha \alpha m_\alpha}\left(l' + \sum_\beta \beta n_\beta\right)\prod_\alpha J_{n_\alpha}(\xi_\alpha) J_{n_\alpha - m_\alpha}(\xi_\alpha)\\ &+\frac{\xi_1}{2} i e^{i\frac{F\tau}{2}} \sum_{l'}\sum_{\{n_\alpha,m_\alpha\}} \Psi_{l'}(0)\Psi^*_{l'+\sum_\alpha \alpha m_\alpha+1}(0) i^{\sum_\alpha m_\alpha} e^{i\frac{F\tau}{2}\sum_\alpha \alpha m_\alpha}\prod_\alpha J_{n_\alpha}(\xi_\alpha) J_{n_\alpha - m_\alpha}(\xi_\alpha)\\ &-\frac{\xi_1}{2} i e^{-i\frac{F\tau}{2}} \sum_{l'}\sum_{\{n_\alpha,m_\alpha\}} \Psi_{l'}(0)\Psi^*_{l'+\sum_\alpha \alpha m_\alpha-1}(0) i^{\sum_\alpha m_\alpha} e^{i\frac{F\tau}{2}\sum_\alpha \alpha m_\alpha}\prod_\alpha J_{n_\alpha}(\xi_\alpha) J_{n_\alpha - m_\alpha}(\xi_\alpha),\end{aligned}$$

where all indices α,β range from 2 to A. In the next step, the recursion and orthogonality relations of Eq. (16) can be employed again to evaluate the sums over n_α and m_α for each α, which finally gives

$$\langle X\rangle_\tau = \sum_l l|\Psi_l(0)|^2 + \sum_{\alpha=1}^A \alpha\xi_\alpha \mathrm{Re}\left[ie^{i\frac{\alpha F\tau}{2}}\sum_l \Psi_l(0)\Psi^*_{l+\alpha}(0)\right] = \langle X\rangle_0 + \sum_{\alpha=1}^A \frac{2t_\alpha}{F}\mathrm{Re}[(e^{i\alpha F\tau}-1)g(\alpha)], \tag{B1}$$

where we have introduced $g(\alpha) := \sum_l \Psi_l(0)\Psi^*_{l+\alpha}(0)$ (see also the recent finding within the nearest-neighbor model [33]). The calculation of $\langle X^2\rangle_\tau$ is more involved but proceeds along the same lines, so we only state the final result:

$$\begin{aligned}\langle X^2\rangle_\tau = \langle X^2\rangle_0 &+ \sum_{\alpha=1}^A 8\frac{t_\alpha^2}{F^2}\sin^2\frac{\alpha F\tau}{2}\{1-\mathrm{Re}[e^{i\alpha F\tau}g(2\alpha)]\} + \sum_{\alpha=1}^A \frac{2t_\alpha}{F}\mathrm{Re}\left[(e^{i\alpha F\tau}-1)\sum_l (2l+\alpha)\Psi_l(0)\Psi^*_{l+\alpha}(0)\right]\\ &+ \sum_{\alpha,\beta=1,\alpha\neq\beta}^A 8\frac{t_\alpha t_\beta}{F^2}\sin\frac{\alpha F\tau}{2}\sin\frac{\beta F\tau}{2}\mathrm{Re}\left[e^{i(\alpha-\beta)\frac{F\tau}{2}}g(\alpha-\beta) - e^{i(\alpha+\beta)\frac{F\tau}{2}}g(\alpha+\beta)\right].\end{aligned} \tag{B2}$$

Now, if we take the initial wave function to be real and symmetric with respect to a site l_0, i.e., $\Psi_{l_0+l}(0) = \Psi_{l_0-l}(0)$, it can be seen that $\sum_l (2l+\alpha)\Psi_l(0)\Psi_{l+\alpha}(0) = 2\langle X\rangle_0 g(\alpha)$, yielding the simplified expressions

$$\begin{aligned}\langle X\rangle_\tau &= \langle X\rangle_0 - \sum_{\alpha=1}^A \frac{4t_\alpha}{F}g(\alpha)\sin^2\frac{\alpha F\tau}{2},\\ \langle X^2\rangle_\tau &= \langle X^2\rangle_0 + \sum_{\alpha=1}^A 8\frac{t_\alpha^2}{F^2}\sin^2\frac{\alpha F\tau}{2}[1-g(2\alpha)\cos(\alpha F\tau)] - \langle X\rangle_0\sum_{\alpha=1}^A \frac{8t_\alpha}{F}g(\alpha)\sin^2\frac{\alpha F\tau}{2}\\ &\quad + \sum_{\alpha,\beta=1,\alpha\neq\beta}^A 8\frac{t_\alpha t_\beta}{F^2}\sin\frac{\alpha F\tau}{2}\sin\frac{\beta F\tau}{2}\left[g(\alpha-\beta)\cos\frac{(\alpha-\beta)F\tau}{2} - g(\alpha+\beta)\cos\frac{(\alpha+\beta)F\tau}{2}\right].\end{aligned}$$

Specializing to the Gaussian wave packet centered at site $l_0 = 0$, we furthermore have $\langle X\rangle_0 = 0$ and the functions $g(\alpha)$ can be evaluated in terms of theta functions using the sum [56]

$$\sum_l e^{-[l^2+(l+\alpha)^2]/(2\sigma)} = e^{-\alpha^2/(4\sigma)}\sqrt{\sigma\pi}\;\vartheta_3\left(\alpha\frac{\pi}{2}, e^{-\sigma\pi^2}\right).$$

This results in Eqs. (18) and (19) of the main text.

[1] F. Bloch, Über die Quantenmechanik der Elektronen in Kristallgittern, Z. Phys. **52**, 555 (1929).

[2] C. Zener, A theory of the electrical breakdown of solid dielectrics, Proc. R. Soc. London, Ser. A **145**, 523 (1934).

[3] J. Feldmann, K. Leo, J. Shah, D. A. B. Miller, J. E. Cunningham, T. Meier, G. von Plessen, A. Schulze, P. Thomas, and S. Schmitt-Rink, Optical investigation of Bloch oscillations in a semiconductor superlattice, Phys. Rev. B **46**, 7252 (1992).

[4] F. Rossi, Bloch oscillations and Wannier-Stark localization in semiconductor superlattices, in *Theory of Transport Properties of Semiconductor Nanostructures*, Electronic Materials Series,

Vol. 4, edited by E. Schöll (Springer, New York, 1998), pp. 283–320.

[5] M. Ben Dahan, E. Peik, J. Reichel, Y. Castin, and C. Salomon, Bloch oscillations of atoms in an optical potential, Phys. Rev. Lett. **76**, 4508 (1996).

[6] S. R. Wilkinson, C. F. Bharucha, K. W. Madison, Q. Niu, and M. G. Raizen, Observation of atomic Wannier-Stark ladders in an accelerating optical potential, Phys. Rev. Lett. **76**, 4512 (1996).

[7] R. Morandotti, U. Peschel, J. S. Aitchison, H. S. Eisenberg, and Y. Silberberg, Experimental observation of linear and nonlinear optical Bloch oscillations, Phys. Rev. Lett. **83**, 4756 (1999).

[8] T. Pertsch, P. Dannberg, W. Elflein, A. Bräuer, and F. Lederer, Optical Bloch oscillations in temperature tuned waveguide arrays, Phys. Rev. Lett. **83**, 4752 (1999).

[9] R. Sapienza, P. Costantino, D. Wiersma, M. Ghulinyan, C. J. Oton, and L. Pavesi, Optical analogue of electronic Bloch oscillations, Phys. Rev. Lett. **91**, 263902 (2003).

[10] P. Cladé, E. de Mirandes, M. Cadoret, S. Guellati-Khélifa, C. Schwob, F. Nez, L. Julien, and F. Biraben, Determination of the fine structure constant based on Bloch oscillations of ultracold atoms in a vertical optical lattice, Phys. Rev. Lett. **96**, 033001 (2006).

[11] B. P. Anderson and M. A. Kasevich, Macroscopic quantum interference from atomic tunnel arrays, Science **282**, 1686 (1998).

[12] G. Roati, E. de Mirandes, F. Ferlaino, H. Ott, G. Modugno, and M. Inguscio, Atom interferometry with trapped Fermi gases, Phys. Rev. Lett. **92**, 230402 (2004).

[13] G. Ferrari, N. Poli, F. Sorrentino, and G. M. Tino, Long-lived Bloch oscillations with bosonic Sr atoms and application to gravity measurement at the micrometer scale, Phys. Rev. Lett. **97**, 060402 (2006).

[14] P. G. Kevrekidis, *The Discrete Nonlinear Schrödinger Equation: Mathematical Analysis, Numerical Computations and Physical Perspectives* (Springer, Berlin, 2009).

[15] G. Gaeta, On a model of DNA torsion dynamics, Phys. Lett. A **143**, 227 (1990).

[16] T. Dauxois, Dynamics of breather modes in a nonlinear "helicoidal" model of DNA, Phys. Lett. A **159**, 390 (1991).

[17] S. Zdravković, Helicoidal Peyrard–Bishop model of DNA dynamics, J. Nonlinear Math. Phys. **18**, 463 (2011).

[18] Y. B. Gaididei, S. F. Mingaleev, P. L. Christiansen, and K. O. Rasmussen, Effects of nonlocal dispersive interactions on self-trapping excitations, Phys. Rev. E **55**, 6141 (1997).

[19] X.-G. Zhao, G. A. Georgakis, and Q. Niu, Photon assisted transport in superlattices beyond the nearest-neighbor approximation, Phys. Rev. B **56**, 3976 (1997).

[20] F. Dreisow, A. Szameit, M. Heinrich, T. Pertsch, S. Nolte, and A. Tünnermann, Second-order coupling in femtosecond-laser-written waveguide arrays, Opt. Lett. **33**, 2689 (2008).

[21] D. Hennig, Next-nearest neighbor interaction and localized solutions of polymer chains, Eur. Phys. J. B **20**, 419 (2001).

[22] N. K. Efremidis and D. N. Christodoulides, Discrete solitons in nonlinear zigzag optical waveguide arrays with tailored diffraction properties, Phys. Rev. E **65**, 056607 (2002).

[23] P. Kevrekidis, B. Malomed, A. Saxena, A. Bishop, and D. Frantzeskakis, Higher-order lattice diffraction: solitons in the discrete NLS equation with next-nearest-neighbor interactions, Phys. D (Amsterdam) **183**, 87 (2003).

[24] A. Szameit, R. Keil, F. Dreisow, M. Heinrich, T. Pertsch, S. Nolte, and A. Tünnermann, Observation of discrete solitons in lattices with second-order interaction, Opt. Lett. **34**, 2838 (2009).

[25] G. Wang, J. P. Huang, and K. W. Yu, Nontrivial Bloch oscillations in waveguide arrays with second-order coupling, Opt. Lett. **35**, 1908 (2010).

[26] F. Dreisow, G. Wang, M. Heinrich, R. Keil, A. Tünnermann, S. Nolte, and A. Szameit, Observation of anharmonic Bloch oscillations, Opt. Lett. **36**, 3963 (2011).

[27] A. Szameit, T. Pertsch, S. Nolte, A. Tünnermann, and F. Lederer, Long-range interaction in waveguide lattices, Phys. Rev. A **77**, 043804 (2008).

[28] A. J. Martínez and M. I. Molina, Diffusion in infinite and semi-infinite lattices with long-range coupling, J. Phys. A: Math. Theor. **45**, 275204 (2012).

[29] H. Fukuyama, R. A. Bari, and H. C. Fogedby, Tightly bound electrons in a uniform electric field, Phys. Rev. B **8**, 5579 (1973).

[30] D. H. Dunlap and V. M. Kenkre, Dynamic localization of a charged particle moving under the influence of an electric field, Phys. Rev. B **34**, 3625 (1986).

[31] M. J. Zhu, X.-G. Zhao, and Q. Niu, Manipulation of band electrons with a rectangular-wave electric field, J. Phys.: Condens. Matter **11**, 4527 (1999).

[32] M. A. Jivulescu and E. Papp, On the dynamic localization conditions for dc–ac electric fields proceeding beyond the nearest-neighbour description, J. Phys.: Condens. Matter **18**, 6853 (2006).

[33] F. Domínguez-Adame, Beyond the semiclassical description of Bloch oscillations, Eur. J. Phys. **31**, 639 (2010).

[34] M. Grifoni and P. Hänggi, Driven quantum tunneling, Phys. Rep. **304**, 229 (1998).

[35] I. L. Garanovich, S. Longhi, A. A. Sukhorukov, and Y. S. Kivshar, Light propagation and localization in modulated photonic lattices and waveguides, Phys. Rep. **518**, 1 (2012).

[36] W. Wang and S. Xiong, Possible first order phase transition in the one-dimensional helical Hubbard model, Phys. Lett. A **156**, 415 (1991).

[37] S.-J. Xiong, Bethe ansatz study of 1+1 dimensional Hubbard model, Z. Phys. B **89**, 29 (1992).

[38] M. Bhattacharya, Lattice with a twist: Helical waveguides for ultracold matter, Opt. Commun. **279**, 219 (2007).

[39] D. Reitz and A. Rauschenbeutel, Nanofiber-based double-helix dipole trap for cold neutral atoms, Opt. Commun. **285**, 4705 (2012).

[40] P. Schmelcher, Effective long-range interactions in confined curved dimensions, Europhys. Lett. **95**, 50005 (2011).

[41] A. V. Zampetaki, J. Stockhofe, S. Krönke, and P. Schmelcher, Classical scattering of charged particles confined on an inhomogeneous helix, Phys. Rev. E **88**, 043202 (2013).

[42] F. H. L. Essler, H. Frahm, F. Göhmann, A. Klümper, and V. Korepin, *The One-Dimensional Hubbard Model* (Cambridge University Press, Cambridge, UK, 2005).

[43] C. J. Pethick and H. Smith, *Bose-Einstein Condensation in Dilute Gases* (Cambridge University Press, Cambridge, UK, 2008).

[44] C. Chin, R. Grimm, P. Julienne, and E. Tiesinga, Feshbach resonances in ultracold gases, Rev. Mod. Phys. **82**, 1225 (2010).

[45] H. D. Cornean, A. Nenciu, and G. Nenciu, Optimally localized Wannier functions for quasi one-dimensional nonperiodic insulators, J. Phys. A: Math. Theor. **41**, 125202 (2008).
[46] L. He and D. Vanderbilt, Exponential decay properties of Wannier functions and related quantities, Phys. Rev. Lett. **86**, 5341 (2001).
[47] A. Trombettoni and A. Smerzi, Discrete solitons and breathers with dilute Bose-Einstein condensates, Phys. Rev. Lett. **86**, 2353 (2001).
[48] S. Greschner, L. Santos, and T. Vekua, Ultracold bosons in zig-zag optical lattices, Phys. Rev. A **87**, 033609 (2013).
[49] A. Dhar, T. Mishra, R. V. Pai, S. Mukerjee, and B. P. Das, Hard-core bosons in a zig-zag optical superlattice, Phys. Rev. A **88**, 053625 (2013).
[50] G. H. Wannier, Wave functions and effective Hamiltonian for Bloch electrons in an electric field, Phys. Rev. **117**, 432 (1960).
[51] G. H. Wannier, Dynamics of band electrons in electric and magnetic fields, Rev. Mod. Phys. **34**, 645 (1962).
[52] T. Hartmann, F. Keck, H. J. Korsch, and S. Mossmann, Dynamics of Bloch oscillations, New J. Phys. **6**, 2 (2004).
[53] I. Gradshteyn and I. Ryzhik, *Table of Integrals, Series, and Products*, 7th ed., edited by A. Jeffrey and D. Zwillinger (Academic, New York, 2007).
[54] M. Holthaus and D. W. Hone, Localization effects in ac-driven tight-binding lattices, Philos. Mag. B **74**, 105 (1996).
[55] A. Szameit, T. Pertsch, S. Nolte, A. Tünnermann, U. Peschel, and F. Lederer, Optical Bloch oscillations in general waveguide lattices, J. Opt. Soc. Am. B **24**, 2632 (2007).
[56] R. Bellmann, *A Brief Introduction To Theta Functions* (Holt, Rinehart and Winston, New York, 1961).
[57] X.-G. Zhao, Dynamic localization conditions of a charged particle in a dc-ac electric field, Phys. Lett. A **155**, 299 (1991).
[58] C. Kittel, *Introduction to Solid State Physics*, 7th ed. (Wiley, New York, 1996).
[59] G. Nenciu, Dynamics of band electrons in electric and magnetic fields: Rigorous justification of the effective Hamiltonians, Rev. Mod. Phys. **63**, 91 (1991).
[60] E. J. Candes and M. B. Wakin, An introduction to compressive sampling, IEEE Signal Process. Mag. **25**, 21 (2008).
[61] X. Andrade, J. N. Sanders, and A. Aspuru-Guzik, Application of compressed sensing to the simulation of atomic systems, Proc. Natl. Acad. Sci. U.S.A. **109**, 13928 (2012).
[62] A. Rauschenbeutel (private communication).
[63] E. Vetsch, D. Reitz, G. Sagué, R. Schmidt, S. T. Dawkins, and A. Rauschenbeutel, Optical interface created by laser-cooled atoms trapped in the evanescent field surrounding an optical nanofiber, Phys. Rev. Lett. **104**, 203603 (2010).
[64] E. Vetsch, S. Dawkins, R. Mitsch, D. Reitz, P. Schneeweiss, and A. Rauschenbeutel, Nanofiber-based optical trapping of cold neutral atoms, IEEE J. Sel. Topics Quantum Electron. **18**, 1763 (2012).
[65] M. Tezuka, A. M. García-García, and M. A. Cazalilla, Destruction of long-range order by quenching of the hopping range in one dimension, Phys. Rev. A **90**, 053618 (2014).
[66] J. Schönmeier-Kromer and L. Pollet, Ground-state phase diagram of the two-dimensional Bose-Hubbard model with anisotropic hopping, Phys. Rev. A **89**, 023605 (2014).
[67] P. Corboz, G. Evenbly, F. Verstraete, and G. Vidal, Simulation of interacting fermions with entanglement renormalization, Phys. Rev. A **81**, 010303 (2010).
[68] T. Lahaye, C. Menotti, L. Santos, M. Lewenstein, and T. Pfau, The physics of dipolar bosonic quantum gases, Rep. Prog. Phys. **72**, 126401 (2009).
[69] K. T. Law and D. E. Feldman, Quantum phase transition between a Luttinger liquid and a gas of cold molecules, Phys. Rev. Lett. **101**, 096401 (2008).
[70] S. Gammelmark and N. T. Zinner, Dipoles on a two-leg ladder, Phys. Rev. B **88**, 245135 (2013).
[71] J. K. Pedersen, D. V. Fedorov, A. S. Jensen, and N. T. Zinner, Formation of classical crystals of dipolar particles in a helical geometry, J. Phys. B: At., Mol. Opt. Phys. **47**, 165103 (2014).